

## Original Paper

# Minerals for wastewater purification: a case study

Anna Maria Cardinale<sup>1</sup> , Cristina Carbone<sup>2</sup>, Marco Fortunato<sup>1</sup> , Ernesto Mesto<sup>3</sup>, Elisabetta Fanizza<sup>4</sup> and Maria Lacalamita<sup>3</sup> 

<sup>1</sup>Department of Chemistry and Industrial Chemistry (DCCI), University of Genoa, Genoa 16146, Italy; <sup>2</sup>Department for the Earth, Environment and Life Sciences (DISTAV), University of Genoa, Genoa 16132, Italy; <sup>3</sup>Earth and Geoenvironmental Sciences Department, University of Bari Aldo Moro, Bari 70125, Italy and <sup>4</sup>Department of Chemistry, University of Bari Aldo Moro, Bari 70125, Italy

### Abstract

Amongst the various strategies studied to reduce polluting agents in water, both from anthropogenic and natural sources, adsorption processes are among the most widespread techniques. Layered double hydroxides (LDH, anionic adsorbents) play a fundamental role in the treatment of industrial wastewater, which often contains both anionic and cationic species. The objectives of the present study were to synthesize a (Mg, Zn) Al-NO<sub>3</sub> LDH, and a composite between the LDH and montmorillonite (Mnt, cationic exchanger), and to test their adsorption capacity for both cationic and anionic pollutants in two different samples of industrial wastewater. The compounds were characterized by means of inductively coupled plasma-atomic emission spectroscopy (ICP-AES), X-ray powder diffraction (XRPD), Fourier-transform infrared (FT-IR) spectroscopy, differential thermal analysis/thermogravimetry (DTA-TG), and transmission electron microscopy (TEM). Results of product yields and extraction performance provided evidence that the synthesized compounds were active in the removal of various kinds of pollutants from real wastewaters. The adsorption capacity, in the case of the removal of cations varied from ~85 to 100% and from ~92 to 100% when the LDH and the LDH-Mnt, respectively, were used. The 56–100% removal of anions was instead obtained for both the adsorbents.

**Keywords:** adsorption; industrial wastewater remediation; ZnMgAl-NO<sub>3</sub> LDH

(Received: 24 July 2024; revised: 16 November 2024; accepted: 18 December 2024)

### Introduction

Water is vital for sustaining life on Earth, and its contamination poses significant risks to both human health and the environment. With global population growth and water contamination worsening, freshwater scarcity is emerging as a major global concern (Hussein, 2018). Various pollutants, both organic and inorganic, can contaminate water, depending on the pollution sources; consequently, the exploration of purification methods is required (Ricky et al., 2022). Comprehensive evaluation of these methods, including their environmental impact assessment (EIA) and compliance with the Sustainable Development Goals of the United Nations 2030 Agenda (particularly the n. 6, Clean Water and Sanitation) is necessary (Fuentes-Bargues, 2018).

Although many metals are essential micronutrients for life at low concentrations, when that concentration is too high, they can be very toxic and potentially do great harm to soil, plants, the human body, and other organisms (Tchounwou et al., 2012). The simultaneous removal of cationic and anionic metals from industrial wastewaters is

considered to be complex as pollutants can compete and interfere with each other (El-Baz et al., 2020).

Adsorption techniques offer promising solutions to these issues as they are able to remove contaminants from water, and the spent adsorbent can be disposed of properly or further applications can be found for it, according to the circular economy (Dehmani et al., 2024; Fortunato et al., 2024). Various adsorbents have been studied and their performances tested (Al-Ghouti et al., 2023; Tewari et al., 2023). Clay minerals and layered double hydroxides (LDH) are among the materials studied for their adsorption capabilities. Clay minerals act mainly as cation exchangers (Liu et al., 2024), while LDH primarily exchange anions and offer advantages compared with other adsorbents, such as ease and cost effectiveness of the synthesis and a good working ability over a wide pH range, from ~3 to 11 (Ardau et al., 2012; Asiabi et al., 2017).

LDH are two-dimensional intercalated compounds with the general formula  $[M^{2+}_{(1-x)}M^{3+}_x(OH)_2]^{x+}(A^{n-})^{x-}\cdot nH_2O$  where  $M^{2+}$  and  $M^{3+}$  represent sites occupied by di- and trivalent cations, respectively;  $A$  indicates the interlayer anions and  $n$  their relative charge; the molar ratio,  $x$ , is usually a value ranging between 0.2 and 0.33. LDH built with  $M^+=Li$  or  $M^{3+}=Al$  cations also have been reported (Britto and Vishnu Kamath, 2011). LDH with simple anions tend to crystallize in two widespread polytypes,  $3R$  ( $R\bar{3}m$  space group) and  $2H$  ( $C2/m$  space group), and may also

**Corresponding author:** Anna Maria Cardinale; Email: [cardinal@chimica.unige.it](mailto:cardinal@chimica.unige.it)

**Cite this article:** Cardinale A.M., Carbone C., Fortunato M., Mesto E., Fanizza E., & Lacalamita M. (2025). Minerals for wastewater purification: a case study. *Clays and Clay Minerals* 73, e10, 1–8. <https://doi.org/10.1017/cmn.2024.45>

be affected by stacking faults and turbostratic disorder (Sławiński et al., 2016). The possibility to tune the composition of the *M* and *A* sites and the ability to intercalate a wide range of different compounds make this class of materials remarkably interesting in a number of research fields that are very different from each other.

Several studies have focused on using LDH for removal from wastewater contaminants and pollutants such as chromate (Cardinale et al., 2020) and phosphate (Zhang et al., 2013). Wang et al. (2021) reviewed the synthesis as well as the application of LDH-based nanocomposites in pollution adsorption.

The purpose of the present case study was to test the adsorbent performance of two synthetic phases, a ternary (Mg,Zn)Al-NO<sub>3</sub> LDH and a composite between the LDH and montmorillonite (Mnt), in the treatment of two real industrial wastewaters with respect to certain pollutants, including metals.

## Materials and methods

### Materials

Aluminum sulfate (Al<sub>2</sub>(SO<sub>4</sub>)<sub>3</sub>·9H<sub>2</sub>O, 99 mass% purity; VWR Chemicals, Leuven, Belgium), zinc nitrate (Zn(NO<sub>3</sub>)<sub>2</sub>·7H<sub>2</sub>O, 99 mass% purity; VWR Chemicals), Mg(NO<sub>3</sub>)<sub>2</sub>·9H<sub>2</sub>O (98.9 mass% purity; VWR Chemicals), and sodium hydroxide (NaOH, >97 mass % purity; Merck, Milano, Italy) were used. Mnt (Kunipia-F) was provided by Kunimine Industries Co., Ltd, Tokyo, Japan. All reactions were carried out in aqueous solvent, using deionized water produced by an ion-exchange unit (M3/M6 Chemical Bürger s.a.s., Genova, Italy).

Two different wastewater samples labeled 'sample1' and 'sample2' (due to confidentiality reasons) were provided by two different industrial plants. The composition of both the samples, as determined by inductively coupled plasma-atomic emission spectroscopy (ICP-AES), is reported in the 'Adsorption results' section.

### Synthesis and characterization

The synthesis of the (MgZn)Al-nitrate LDH, through the co-precipitation approach under an inert atmosphere, was carried out starting from the method proposed by Yi et al. (2013), although small variations were necessary due to the absence of Mnt in the synthesis; furthermore, the entire synthesis process was carried out in closed vessels under argon flow. The nitrate salts of the three metals were weighed to obtain a 150 mL aqueous solution containing 0.033 mol L<sup>-1</sup> Mg<sup>2+</sup>, 0.099 mol L<sup>-1</sup> Zn<sup>2+</sup>, and 0.066 mol L<sup>-1</sup> Al<sup>3+</sup>. These concentrations gave the desired metal ratios. The water for the solution was deionized and previously boiled to avoid the presence of carbonate. The salts were dissolved at room temperature under mechanical stirring. The solution was then placed in a three-necked flask and the pH was stabilized in the range of 9–11 by adding NaOH (1 mol L<sup>-1</sup>) dropwise at room temperature under stirring. An initial estimate of the volume of NaOH solution required to stabilize the pH was approximately equal to three times the total moles of the metals. The reaction product (solution with the solid precursor of LDH) was transferred into a dark glass bottle and aged in an oven at 60°C for 3 days under an inert atmosphere. The LDH was recovered from the solution by centrifugation at 7000 rpm (5752 x g) for 10 min, washed repeatedly with water, and dried in an oven at 60°C for 24 h.

Based on the findings of Yi et al. (2013), the LDH-Mnt composite was prepared with an amount of Mnt equal to 50% of the mass of the

divalent metals. This ratio was chosen to achieve good crystallinity and surface charge density of the synthesized composite. The method, proposed by Yi et al. (2013), involved an initial dispersion of Mnt in 200 mL of H<sub>2</sub>O inside a three-necked flask, under mild mechanical stirring and argon flow. The pH was adjusted to a value between 2 and 5 with a few drops of HNO<sub>3</sub> solution, which eliminated any traces of carbonate in the system. The acidic pH also inhibited the possible precipitation of metal hydroxides. The synthesis was repeated by increasing the lower limit of the permitted pH range to 3 and adjusted to a value between 3 and 5 to prevent the co-precipitation of additional products (Mg-Mnt, Mg(OH)<sub>2</sub>, Al(OH)<sub>3</sub>, Mg(OH)<sub>2</sub>-Mnt and Al(OH)<sub>3</sub>-Mnt).

Once the pH was stabilized (between 2 and 5, or 3 and 5), the metal salts were added and the mixture was heated to 70°C under vigorous mechanical stirring (~1000 rpm) for 24 h. After this time, 1 M NaOH was added slowly using a peristaltic pump. Both the gas flow and the stirring were left unchanged. The change in pH was monitored continuously up to a value between 9 and 11 and stable over 30 min. The mixture of solid precursor and supernatant solution was recovered by transferring it directly from the flask and into a glass bottle and left to age in an oven for 2 days at 60°C. The resulting solid-phase composite ('LDH-Mnt\_1' sample obtained at pH2–5; 'LDH-Mnt\_2' sample obtained at pH3–5) was separated from the solution by centrifugation at 7000 rpm (5752 x g) for 10 min, washed repeatedly with water and dried in an oven at 60°C for 24 h.

All the synthesized samples were characterized to determine their mineralogical and elemental composition, structure, and morphology using ICP-AES, X-ray powder diffraction (XRPD), Fourier-transform infrared (FTIR) spectroscopy, differential thermal analysis/thermogravimetry (DTA-TG), and transmission electron microscopy (TEM). The ICP-AES measurements were performed using an axially viewed Varian (Springvale, Australia) Vista PRO instrument.

The XRPD analyses were carried out on the LDH, Mnt, and LDH-Mnt samples after grinding by hand in an agate mortar up to 120-mesh. Samples were top-loaded in the sample holder, then placed in a Panalytical Empyrean X-ray powder diffractometer equipped with a Cu target ( $\lambda=1.5406$  Å) operating at 40 mA and 40 kV. XRD patterns were acquired in step-scan mode over the 3–70°2 $\theta$  range, with a step size of 0.026°2 $\theta$  and a measuring time of 348 s step<sup>-1</sup>. The XRPD pattern of the LDH-Mnt\_1 sample was measured in the 5–90°2 $\theta$  range using an X'Pert MPD (Philips, Almelo, Netherlands) diffractometer equipped with a Cu target and step scanned at 0.001°2 $\theta$  and 50 s step<sup>-1</sup>. The diffraction data obtained were indexed by comparison with XRD patterns available in the literature (Villarks and Cenzual, 2017), and the lattice parameters of the phases were calculated using the LATCON program (Schwarzenbach, 1975).

The FTIR spectra were obtained in the 4000–600 cm<sup>-1</sup> wavenumber range using a Spectrum 65 FT-IR Spectrometer (PerkinElmer, Waltham, MA, USA) equipped with a KBr beam-splitter and a DTGS detector using an ATR accessory with a diamond crystal. All the samples were analyzed in the solid state after grinding and mixing with solid KBr.

### Samples

The TG/DTA analysis was performed using a LabsysEvo 1600-Setaram instrument; ~20 mg of powdered sample was placed in an open alumina crucible and heated from 30 to 1250°C at 10°C min<sup>-1</sup>, under a flowing Ar atmosphere at 60 mL min<sup>-1</sup>.

The TEM analysis was conducted using a JEOL Jem-1011 microscope operating at an accelerating voltage of 100 kV. The TEM images were captured using a Quemesa Olympus CCD 11 Mp camera. Samples were prepared by drop-casting MgZnAl-LDH and MgZnAl-Mnt suspensions in methanol onto a carbon-coated TEM grid and allowing the solvent to evaporate. The pH was monitored with a pH-meter pH/ORP/ISE single channel benchtop meter-HI3221 (Hanna Instruments, Woonsocket, RI, USA).

### Pollutant adsorption tests

The adsorption capacity of the two synthesized materials was tested for different pollutants (both cationic and anionic) present in two different industrial wastewater samples. According to results obtained in previous work (Cardinale et al., 2023) for both solid adsorbents, 1 g of the compound was added to 100 mL of wastewater in which the pH was kept in the range  $5.0 \pm 0.3$  by adding dropwise an aqueous solution of  $0.5 \text{ mol L}^{-1}$  NaOH.

Batch equilibration tests were carried out in a rotary shaker at 15 rpm for 24 h. After adsorption, the solid was recovered by centrifugation at 5000 rpm, washed with deionized water and finally dried in an oven at  $60^\circ\text{C}$ . The residual metal concentration in the solution was determined by ICP-AES.

## Results

### X-ray diffraction

The peak positions from XRPD patterns of Mnt and LDH (Fig. 1A) and of the two LDH-Mnt composites synthesized at different pH values (Fig. 1B) are listed in Table 1.

With regard to the Mnt sample, the measured peak positions were similar to those found for other Mnt (Viani et al., 2002). In particular, a well-defined first-order (001) reflection at a basal spacing of 11.82 Å was observed. The interlayer spacing of Mnt is a function of the hydration state and of the radii of the interlayer cations (Chalghaf et al., 2013). Specifically, the  $d_{001}$  value in the XRD pattern ranging from 12.29 to 15.53 Å was ascribed to unhydrated Mnt interlayers, whereas  $d_{001}$  in the ranges 11.6–12.9, 14.9–15.7, and 18–19 Å were associated with monohydrated (1W,

**Table 1.** Peak positions of the XRPD patterns in Fig. 1

Mnt		LDH		LDH-Mnt_1		LDH-Mnt_2	
(°2θ)	d (Å)	(°2θ)	d (Å)	(°2θ)	d (Å)	(°2θ)	d (Å)
7.48	11.82	11.61	7.65	5.69	15.53	5.39	16.41
19.87	4.47	20.25	4.45	11.00	8.07	10.74	8.24
28.42	3.14	23.25	3.89	16.13	5.54	16.14	5.49
34.86	2.57	34.74	2.70	20.00	4.50	19.80	4.48
54.10	1.70	39.22	2.30	20.10	4.48	25.78	3.46
62.08	1.50	46.47	2.12	35.40	2.66	29.44	3.03
		60.32	1.77	54.35	1.90	30.97	2.89
		61.68	1.50	60.95	1.76	34.78	2.58
				60.80	1.76	60.49	1.53
						61.90	1.50

i.e. 1 layer of water molecules), bihydrated (2W), and trihydrated (3W) states. In the present case study, the interlayer spacing for the pristine Mnt indicates that it was in the monohydrated state.

In the pattern of the MgZnAl-LDH sample, three main reflections at 11.61, 23.35, and  $34.74^\circ 2\theta$  corresponding to basal reflections  $d_{003}$  7.65,  $d_{006}$  3.89, and  $d_{012}$  2.70 Å, respectively, were revealed. Additional peaks at 20.25, 39.22, 46.47, 60.32, and  $61.68^\circ 2\theta$  ( $d=4.45$ , 2.30, 2.12, 1.77, and 1.50 Å, respectively) were also identified as reported in the literature (Lin et al., 2017; Bakr et al., 2018). The asymmetric  $00l$  and  $0kl$  reflections, e.g. (003) at 7.65 Å, (012) at 2.70 Å, and (015) at 2.30 Å, are typical features of diffraction patterns of sheet minerals affected by turbostratic disorder along the  $c^*$  axis (Rits et al., 1984). The calculated lattice parameters of the LDH show values ( $a=3.044(6)$  Å,  $c=23.100(9)$  Å, and  $V=185.36$  Å<sup>3</sup>) very close to those reported in the literature for samples with similar compositions (Cocheci et al., 2010).

Regarding the LDH-Mnt composites, the XRPD patterns (Fig. 1B) were consistent with those reported by Yi et al. (2013). The main difference between the two synthesized compounds was in the position of the first peak, which was

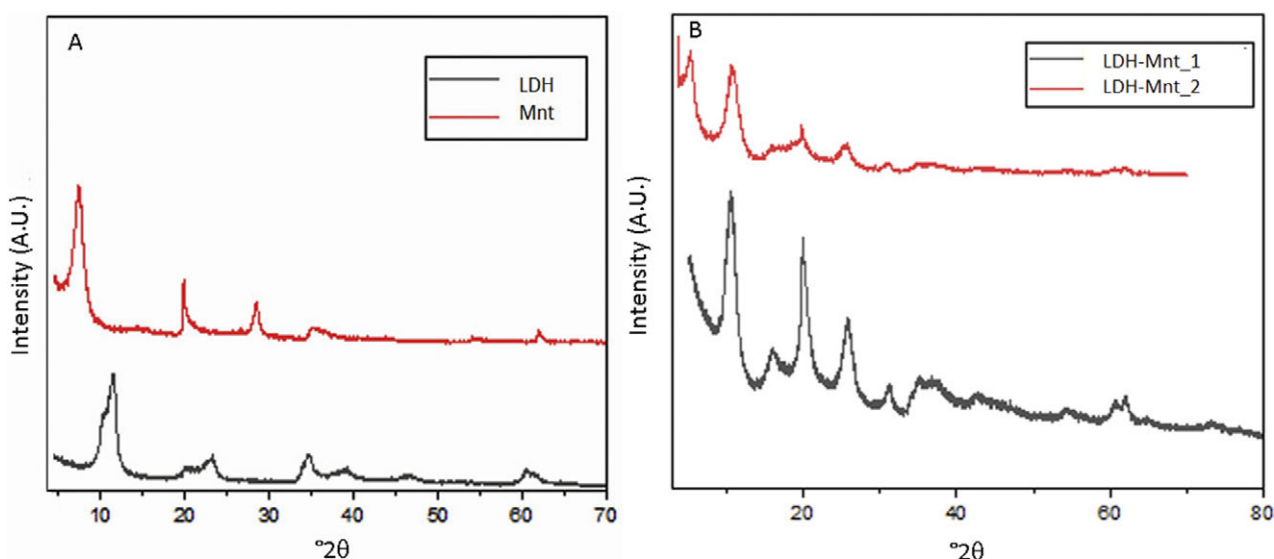


**Figure 1.** XRPD patterns of the samples: (A) LDH (black line) and Mnt (red line); (B) LDH-Mnt\_1 (black line) and LDH-Mnt\_2 (red line).

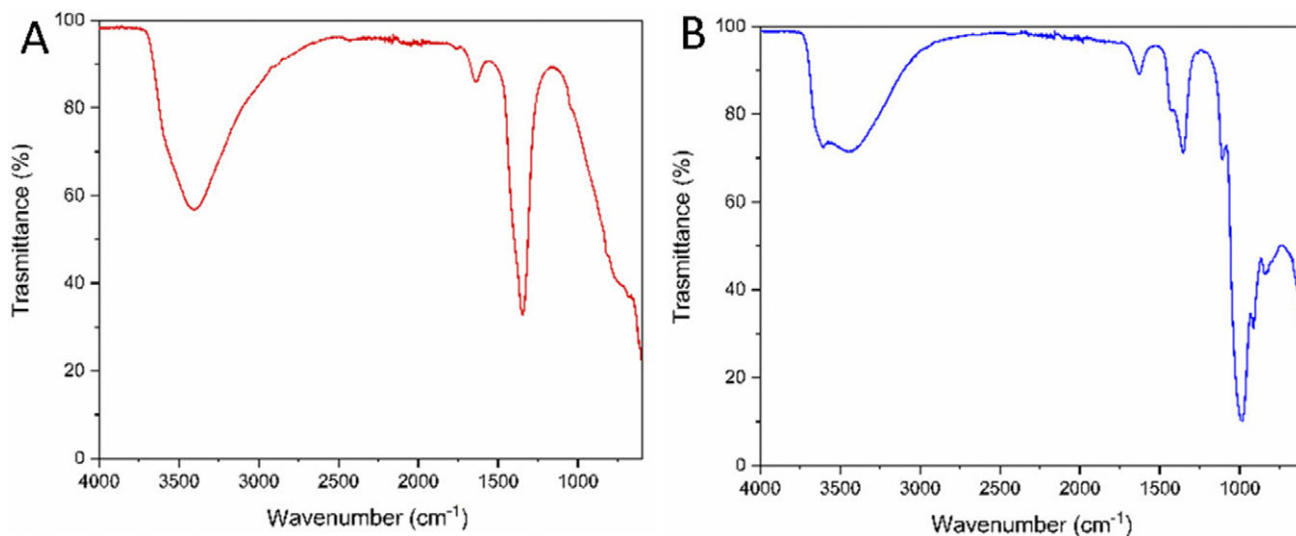


**Figure 2.** Infrared spectra of the samples: (A) LDH and (B) LDH-Mnt.

centered at  $d=15.53$  and  $16.41$  Å in the LDH-Mnt\_1 and LDH-Mnt\_2 samples, respectively.

### Infrared spectroscopy

The infrared spectrum of the MgZnAl-LDH (Fig. 2A) revealed the typical broad band centered at  $3400\text{ cm}^{-1}$  related to O–H stretching; a band at  $1636\text{ cm}^{-1}$  assigned to  $\text{H}_2\text{O}$  bending vibrations (Bakr et al., 2018) or to the carbonyl stretching (Jiang et al., 2019), and a narrow band at  $1346\text{ cm}^{-1}$  pertaining to the N=O stretching vibrations of the nitrate anion.

The IR spectrum obtained for the composite material (Fig. 2B) showed a broad absorption at high wavenumber, including two signals centered at  $3607$  and  $3448\text{ cm}^{-1}$  due to the stretching vibrations of the hydroxyl groups and H–O–H adsorbed water, respectively. The band at  $1628\text{ cm}^{-1}$  derives from the bending of adsorbed  $\text{H}_2\text{O}$ . The two partially overlapped peaks at  $\sim 1429$  and  $1452\text{ cm}^{-1}$  confirmed the presence of nitrate, whereas the peak at  $992\text{ cm}^{-1}$  (and the following at lower wavenumber) pertains to vibrations of the tetrahedral framework.

### Thermal analysis

The thermal behavior of the LDH (Fig. 3A) revealed a typical mass-loss trend of the LDH: a first step in the temperature range  $30\text{--}218^\circ\text{C}$  due to the loss of adsorbed and structural water (13.3 mass%); a second mass loss of 13.7 mass% caused by the dehydroxylation of the brucite layers in the range  $218\text{--}391^\circ\text{C}$ ; and an 8.7 mass% loss at  $T>391^\circ\text{C}$  due to the interlayer nitrate anion decomposition (Lahkale et al., 2018; Fortunato et al., 2024).

The thermal analysis of the composite (Fig. 3B) showed that the total mass loss occurred in two steps: 6.3% in the range  $30\text{--}200^\circ\text{C}$ , which depends on the loss of  $\text{H}_2\text{O}$  without structure collapse (Jiang et al., 2019); 16.9% related to both the interlayer nitrate anion decomposition and the dehydroxylation of the brucite layers ( $222<T<600^\circ\text{C}$ ). The total mass loss was 23.2%.

### Transmission electron microscopy

For a deeper understanding of the morphology of the LDH-Mnt composite, a TEM investigation was performed. The sample

consisted of aggregations of LDH particles (Fig. 4) dispersed within the Mnt lamellae. The size and shape of the LDH particles were affected by the synthesis conditions (Wijitwongwan et al., 2019). They appeared as large ( $\sim 100\text{ nm}$ ) regular hexagons when produced by hydrothermal processes whereas mechanochemical methods produced ultrafine ( $\sim 10\text{--}25\text{ nm}$ ) and irregular particles with hollow interiors and which did not nucleate on the Mnt surface. TEM images of the LDH-Mnt particles showed structures slightly larger than  $50\text{ nm}$  entrapped within a matrix, and the appearance of a circular texture probably ascribed to inclusion of water.

### Adsorption results

The adsorption tests were conducted on two wastewater samples that originated from different industrial processes and contained different pollutants. The two wastewaters were treated with both synthesized composites, as described in the ‘Materials and methods’ section. The composites removed similar amounts of pollutants, as shown by the ICP data (Table 2) on the metal concentrations before and after the treatment, as well as by the adsorption capacity  $q_e$  ( $\text{mg g}^{-1}$ ) for each adsorbed polluting species in the solid substrate, expressed as:

$$q_e = \frac{V(C_0 - C_e)}{m}$$

where  $m$  is the mass of sorbent used in a volume  $V$  of liquid,  $C_0$  is the initial concentration ( $\text{mg L}^{-1}$ ) of pollutant, and  $C_e$  is the concentration of pollutant in the liquid phase in equilibrium with the adsorbed species. Also listed in Table 2 is the fraction,  $r$ , of the initial concentration of pollutant removed by the composite, calculated by:

$$r = \frac{(C_0 - C_e)}{C_0} \times 100$$

Sample 1 consisted of several cations (Cd, Fe, Mn, Ni, Zn) and Se in anionic form. Treatment of this wastewater with LDH removed 85–100% of all metals except 72% for Se. This level of performance, except for Se, was considered to be satisfactory. When sample 1 was treated with LDH-Mnt, the extent of removal of Cd, Fe, Mn, and Zn decreased slightly but remained at  $>90\%$ . On the contrary, the

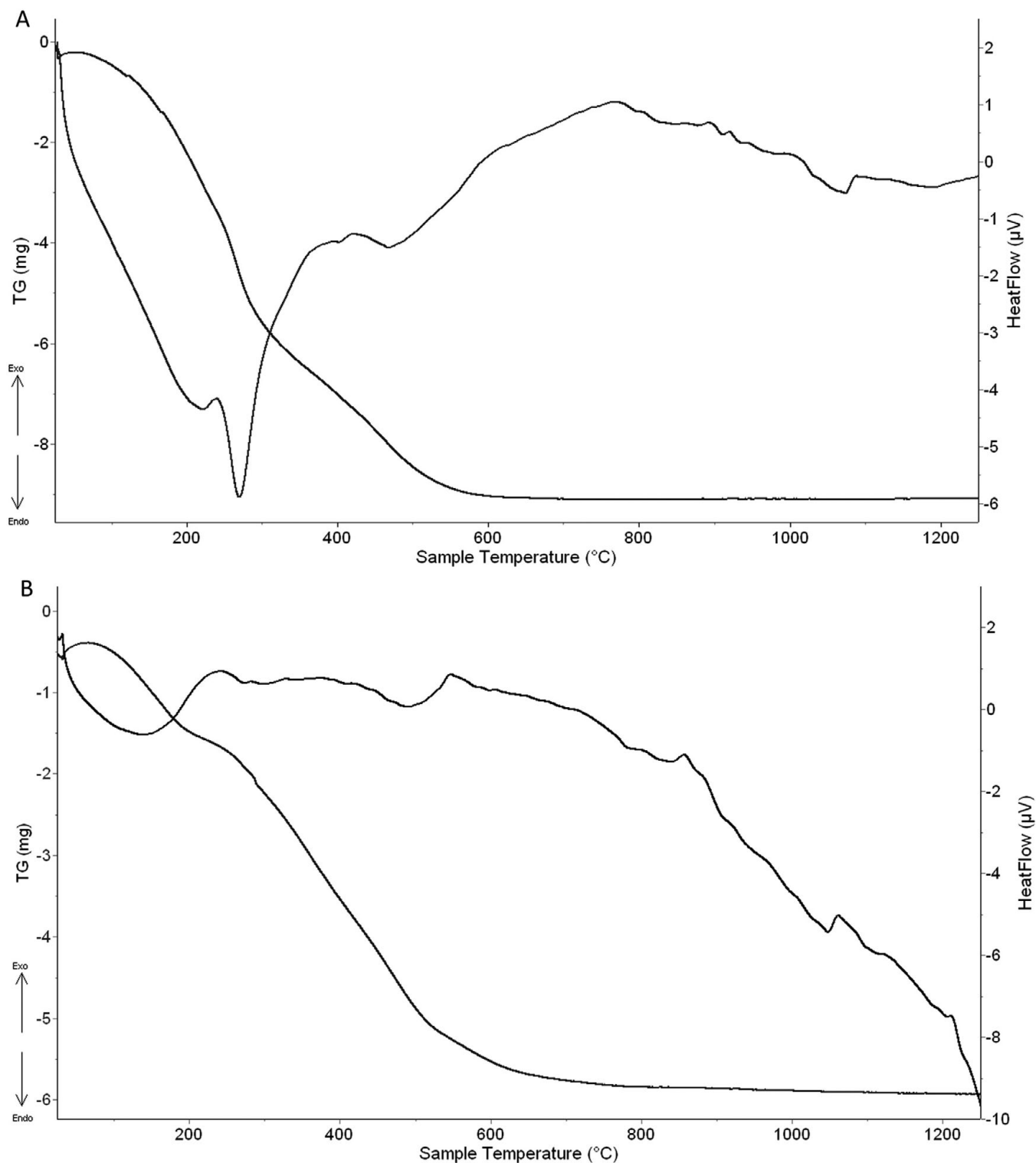


**Figure 3.** TG and heat-flow curves of: (A) LDH and (B) LDH-Mnt samples. Up and down arrows refer to exothermic and endothermic peaks, respectively.

removal of Ni increased and that of Se decreased from 72 to 56%, thus remaining unsatisfactory. These results may be explained by considering that the main adsorption process was due to cation exchange between the octahedral cations (Mg, Al, Zn) in the brucite layers of the LDH and the Cd, Fe, Mn, Ni, and Zn cations dissolved in the wastewater due to similarities in their ionic radii (Shannon and Shannon, 1976). Therefore, the reduced effectiveness of

LDH-Mnt compared with the pure LDH may be due to a lower extent of cation substitution between the contaminants in the solution and the LDH layer. Regarding the selenium, its lower affinity for the interlayer may depend on the pH of the solution which should be tuned to remove the nitrate, de-laminate the LDH and promote the intercalation of the selenium as previously reported by Timmer et al. (2010).

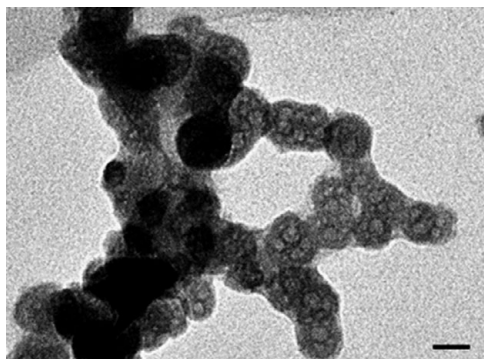


**Figure 4.** TEM image (scale bar = 50 nm) of LDH-Mnt composites.

Sample2 contains fewer pollutants than sample1: two cations (Cu, Fe) and one anion ( $\text{CrO}_4^{2-}$ ). Both the LDH and the LDH-Mnt composite showed comparable behavior toward chromate removal, while LDH had a better affinity toward Cu and Fe. Again, this difference may depend on the exchange mechanism between Cu and Mg due to the similarity in their ionic radii (73 and 72 pm, respectively). The Cu-Mg substitution has already been proposed for Mg-Al LDHs (González et al., 2014; Shannon and Shannon, 1976.). However, other mechanisms (e.g. interaction between Cu and  $\text{OH}^-$  functional groups, surface complexation, and  $\text{Me}(\text{OH})_2$  precipitation on the surface of the composite) should not be excluded completely (Liang et al., 2013).

Regarding the uptake of Fe, no clear behavior for the interaction between the adsorbents and the two wastewaters was observed. The occurrence of interfering ions may explain the different amounts of uptake of the same ion from wastewater with different overall composition.

## Discussion

The XRD results obtained indicate that the pH plays a role in the synthesis of the LDH-Mnt composite. Indeed, the LDH-Mnt\_2 sample showed a  $d_{001}=16.41 \text{ \AA}$  which is the value expected for the LDH-Mnt-50% compound (i.e. Mnt = 50% of the mass of the divalent metals) as also found by Yi et al. (2013). This  $d$  spacing results from the sum of the thickness of a Mnt layer ( $\sim 10 \text{ \AA}$ ), a LDH layer ( $\sim 4.9 \text{ \AA}$ ), and the diameter of the Na ion ( $\sim 2 \text{ \AA}$ ). The LDH-Mnt\_1 sample, instead, exhibited a  $d_{001}=15.53 \text{ \AA}$  which is

**Table 3.** Legal limits in Italy of concentrations of selected metals for disposal in surface water, drainage systems, and soil (Annex 5, part 3, 'Legislative Decree' no. 152 of April 4th, 2006, Italy).

Element	Surface water (ppm)	Drainage system (ppm)	Soil (ppm)
Cd(II)	0.02	0.02	*
Cr(VI)	0.2	0.2	*
Cu(II)	0.1	0.4	0.1
Fe(III)	2.0	4.0	2.0
Mn(II)	2.0	4.0	0.2
Ni(II)	2.0	4.0	0.2
Se(IV)	0.03	0.03	0.002
Zn(II)	0.5	1.0	0.5

\*Not allowed.

compatible with the  $d$ -spacing of LDH-Mnt-70% ( $d_{001}=15.55 \text{ \AA}$ ; Yi et al. 2013) as well as Mg-Mnt ( $d_{001}=15.50 \text{ \AA}$ ; Nanzyo and Kanno, 2018),  $\text{Mg}(\text{OH})_2$ -Mnt ( $d_{001}=15.56 \text{ \AA}$ ; Yi et al., 2013 and references therein), and  $\text{Al}(\text{OH})_3$ -Mnt ( $d_{001}=15.52 \text{ \AA}$ ; Yi et al., 2013 and references therein). Actually, the procedure that was used may also have involved the coprecipitation of  $\text{Mg}(\text{OH})_2$  and  $\text{Al}(\text{OH})_3$  (see Yi et al., 2013). However, no evidence of the characteristic peaks of these phases ( $d_{001}=4.77 \text{ \AA}$  for  $\text{Mg}(\text{OH})_2$  (Zigan, 1967);  $d_{002}=4.88 \text{ \AA}$  for  $\text{Al}(\text{OH})_3$  (Balan et al., 2006)) were found in the collected patterns (Fig. 1B; Table 1).

Overall, both synthesized materials had good adsorption capacities, which in the case of the removal of cations varied from  $\sim 85$  to 100% and from  $\sim 92$  to 100% when the LDH and the LDH-Mnt, respectively, were used. The 56 to 100% removal of anions was instead observed for both the adsorbents. Similar values were obtained previously when zeolite, LDH, and a composite formed by zeolite and LDH were used in the treatment of the wastewater from the petroleum industry (Bezerra et al., 2019).

The results of the present study may also be discussed by referring to the legal limits in Italy for concentrations of the target metals for disposal in surface water, drainage systems, and soil (Table 3).

The Cr(VI) residual concentration in sample2 allows disposal in surface waters and drainage systems if treated with the LDH only;

**Table 2.** Metal-pollutant concentrations before and after treatment with LDH and LDH-Mnt

Element	Sample1						Sample2		
	Cd(II)	Fe(III)	Mn(II)	Ni(II)	Se(IV)	Zn(II)	Cr(VI)	Cu(II)	Fe(III)
$C_0$ (ppm)	7.30	0.11	16.30	0.20	0.18	53.00	86.60	1.39	0.38
LDH									
$C_e$ (ppm)	0.03	0.00	0.04	0.03	0.05	0.00	0.02	0.00	0.04
$q_e$ ( $\text{mg g}^{-1}$ )	0.73	0.01	1.63	0.02	0.01	5.30	8.66	0.14	0.03
$r$	99.6	100	99.8	85	72	100	100	100	89.5
LDH-Mnt									
$C_e$ (ppm)	0.16	0.01	1.37	0.00	0.08	0.40	0.08	0.00	0.00
$q_e$ ( $\text{mg g}^{-1}$ )	0.71	0.01	1.50	0.02	0.01	5.26	8.65	0.14	0.04
$r$	97.8	90.9	91.6	100	55.6	99.2	99.9	100	100

Initial concentration,  $C_0$ ; equilibrium solution concentration,  $C_e$ ; amount in the solid phase,  $q_e$ ; and fraction,  $r$ , removed from solution.

similar considerations pertain to Mn and Cd (sample1). Even if the concentrations of Ni and Fe in the wastewater were low, the adsorption process reduced the amounts present further. A significant reduction of the concentration of Zn (sample1) and Cu (sample2) was obtained when both adsorbents were used. The small initial Se concentration, even after treatment, still remained slightly above the legal limits for surface waters and drainage systems.

## Conclusions

The use of LDH as adsorbent material of potentially toxic elements offers interesting prospects in the field of wastewater remediation and, more generally, in the view of the circular economy, as these materials can be even more effective after their use in the adsorption processes, thus mitigating the challenges and costs associated with the regeneration of the adsorbent and the proper disposal of the pollutants. This approach, effectively combining remediation and recovery, may be implemented at larger-scale in industrial plants.

The results of the present study highlight that the synthesis of LDH and LDH-Mnt is simple, has a good yield and is sustainable. According to inherent safety guidelines, no reagents hazardous to health or the environment were employed. The synthesis is pH-dependent as slight changes in the pH values lead to the crystallization of adsorbents with slightly different structural features. These aspects, however, do not affect the effectiveness of the metals recovery when the adsorbents are contacted with real wastewater solutions. In the applied experimental conditions, the adsorption capacity of the LDH and LDH-Mnt composites toward the cations were found whereas a tuning of the experimental parameters (pH; contact time; etc.) deserves to be further investigated to optimize the adsorption of such anions. These experimental parameters have been demonstrated to be effective in the enhancement of the sorbent performance (Wang et al., 2021). In addition, future experiments on model solutions containing a selection of the contaminants in industrial wastewater may shed light on the possible interactions among the pollutants.

Finally, the feasibility to apply the synthesized composites ((Mg, Zn)Al-NO<sub>3</sub> LDH; LDH-Mnt) for the uptake of toxic metals from real solutions contributes to the research on the development of innovative and eco-friendly materials for the reutilization of wastewaters at industrial scale.

**Author contribution.** Conceptualization: A.M. Cardinale and C. Carbone; methodology: A.M. Cardinale, C. Carbone and E. Mesto; software: M. Fortunato, E. Mesto; validation: E. Mesto, A.M. Cardinale and M. Lacalamita; investigation: A.M. Cardinale, C. Carbone, E. Fanizza and E. Mesto; resources: A.M. Cardinale, C. Carbone and E. Mesto; data curation: A.M. Cardinale, E. Fanizza and E. Mesto; writing – original draft preparation: A.M. Cardinale and M. Fortunato; writing – review and editing: E. Mesto and Maria Lacalamita.; visualization: A.M. Cardinale, E. Mesto and M. Lacalamita; supervision: A.M. Cardinale, E. Mesto and C. Carbone; project administration: A.M. Cardinale. All authors have read and agreed to the published version of the manuscript.

**Acknowledgements.** Two anonymous referees are gratefully acknowledged for their insightful suggestions.

**Financial support.** This research received no external funding.

**Competing interest.** There are no competing interests to declare.

**Data availability statement.** The data presented in this study are available on request from the corresponding author.

## References

- Al-Ghouthi, M.A., Ashfaq, M.Y., Khan, M., Al Disi, Z., Da'na, D.A., & Shoshaa, R. (2023). State-of-the-art adsorption and adsorptive filtration based technologies for the removal of trace elements: a critical review. *Science of the Total Environment*, 895, 164854.
- Arda, C., Frau, F., Dore, E., & Lattanzi, P. (2012). Molybdate sorption by Zn-Al sulphate layered double hydroxides. *Applied Clay Science*, 65–66, 128–133.
- Asiabi, H., Yamini, Y., & Shamsayei, M. (2017). Highly selective and efficient removal of arsenic (V), chromium (VI) and selenium (VI) oxyanions by layered double hydroxide intercalated with zwitterionic glycine. *Journal of Hazardous Materials*, 339, 239–247.
- Bakr, A.A., Sayed, N.A., Salama, T.M., Ali, I.O., Gayed, R.R.A., & Negm, N.A. (2018). Potential of Mg–Zn–Al layered double hydroxide (LDH)/montmorillonite nanocomposite in remediation of wastewater containing manganese ions. *Research on Chemical Intermediates*, 44, 389–405.
- Balan, E., Lazzeri, M., Morin, G., & Mauri, F. (2006) First-principles study of the OH-stretching modes of gibbsite. *American Mineralogist*, 91, 115–119.
- Bezerra, B.G.P., Bieseki, L., da Silva, D.R., & Pergher, S.B.C. (2019). Development of a zeolite A/LDH composite for simultaneous cation and anion removal. *Materials*, 12, 661–673.
- Britto, S., & Vishnu Kamath, P. (2011). Polytypism in the lithium–aluminum layered double hydroxides: the [LiAl<sub>2</sub>(OH)<sub>6</sub>]<sup>+</sup> layer as a structural synthon. *Inorganic Chemistry*, 50, 5619–5627.
- Cardinale, A.M., Carbone, C., Consani, S., Fortunato, M., & Parodi, N. (2020). Layered double hydroxides for remediation of industrial wastewater from a Galvanic plant. *Crystals*, 10, 443. <https://doi.org/10.3390/cryst10060443>
- Cardinale, A.M., Carbone, C., Molinari, S., Salviulo, G., & Ardini, F. (2023). MgAl-NO<sub>3</sub> LDH: adsorption isotherms and multivariate optimization for Cr (VI) removal. *Chemistry*, 5, 633–645. <https://doi.org/10.3390/chemistry5010045>
- Chalghaf, R., Oueslati, W., Ammar, M., Rhaiem, H. B., & Amara, A.B.H. (2013). Effect of temperature and pH value on cation exchange performance of a natural clay for selective (Cu<sup>2+</sup>, Co<sup>2+</sup>) removal: equilibrium, sorption and kinetics. *Progress in Natural Science: Materials International*, 23, 23–35.
- Cochechi, L., Barvinschi, P., Pode, R., Seftel, E.-M., & Popovici, E. (2010) Chromium (VI) ion removal from aqueous solutions using a Zn-Al-type layered double hydroxide. *Adsorption Science & Technology*, 28, 270–278.
- Dehmani, Y., Ba Mohammed, B., Oukhrif, R., Dehbi, A., Lamhasni, T., Brahmi, Y., El-Kordy, A., Franco, D.S.P., Georgin, J., Lima, E.C., Alrashdi, A.A., Tijani, N., & Abouarnadasse, S. (2024). Adsorption of various inorganic and organic pollutants by natural and synthetic zeolites: a critical review. *Arabian Journal of Chemistry*, 17, 105474.
- El-Baz, A.A., Hendy, I.A., Dohdoh, A.M., & Srour, M.I. (2020). Adsorption technique for pollutants removal; current new trends and future challenges – a review. *The Egyptian International Journal of Engineering Sciences and Technology*, 32, 1–24.
- Fortunato, M., Reverberi, A. Pietro, Fabiano, B., & Cardinale, A.M. (2024). Thermal evolution of NiFe-NO<sub>3</sub> LDH and its application in energy storage systems. *Energies*, 17, 1035–1047.
- Fuentes-Bargues, J.L. (2018). Review of the environmental impact assessment process of wastewater treatment plants in Spain. *Environment Protection Engineering*, 44, 23–41.
- González, M.A., Pavlovic, I., Rojas-Delgado, R., & Barriga, C. (2014). Removal of Cu<sup>2+</sup>, Pb<sup>2+</sup> and Cd<sup>2+</sup> by layered double hydroxide-humate hybrid. *Sorbate and sorbent comparative studies*. *Chemical Engineering Journal*, 254, 605–611.
- Hussein, H. (2018). Lifting the veil: unpacking the discourse of water scarcity in Jordan. *Environmental Science and Policy*, 89, 385–392.
- Jiang, D.B., Jing, C., Yuan, Y., Feng, L., Liu, X., Dong, F., Dong, B., & Zhang, Y.X. (2019). 2D-2D growth of NiFe LDH nanoflakes on montmorillonite for cationic and anionic dye adsorption performance. *Journal of Colloid and Interface Science*, 540, 398–409.
- Lahkale, R., Elhatimi, W., Sadik, R., Bouragba, F.Z., Lebbar, N., Elmelouky, A., Mortadi, A., & Sabbar, E. (2018). Nitrate-intercalated Mg1-xAlx-layered double hydroxides with different layer charges (x): preparation, characterization, and study by impedance spectroscopy. *Applied Clay Science*, 158, 55–64.
- Liang, X., Zang, Y., Xu, Y., Tan, X., Hou, W., Wang, L., & Sun, Y. (2013). Sorption of metal cations on layered double hydroxides. *Colloids and Surfaces A: Physicochemical and Engineering Aspects*, 433, 122–131.

- Lin, C.H., Chu, H.L., Hwang, W.S., Wang, M.C., & Ko, H.H. (2017). Synthesis and optical properties of Mg-Al layered double hydroxides precursor powders. *AIP Advances*, 7, 125005–125016.
- Liu, X., Laipan, M., Zhang, C., Zhang, M., Wang, Z., Yuan, M., & Guo, J. (2024). Microbial weathering of montmorillonite and its implication for Cd (II) immobilization. *Chemosphere*, 349, 140850–140862.
- Nanzyo, H., & Kanno, M. (2018). *Inorganic Constituents in Soil*, 188 pp. Springer Nature Singapore Pte Ltd.
- Ricky, R., Shanthakumar, S., Ganapathy, G.P., & Chiampo, F. (2022). Zero liquid discharge system for the tannery industry – an overview of sustainable approaches. *Recycling*, 7, 31–48.
- Rits, V.A.D., Plançon, A., Sakharov, B.A., Besson, G., Tshipursky, S.I., & Tchoubar, C. (1984). Diffraction effects calculated for structural models of K-saturated montmorillonite containing different types of defects. *Clay Minerals*, 19, 541–561.
- Schwarzenbach, D. (1975). *Program LATCON*, University of Lausanne, Switzerland.
- Shannon, R.D., & Shannon, R.D. (1976) Revised effective ionic radii and systematic studies of interatomic distances in halides and chalcogenides. *Acta Crystallographica*, 32, 751–767.
- Sławiński, W.A., Sjästad, A.O., & Fjellvåg, H. (2016). Stacking faults and polytypes for layered double hydroxides: what can we learn from simulated and experimental X-ray powder diffraction data? *Inorganic Chemistry*, 55, 12881–12889.
- Tchounwou, P.B., Yedjou, C.G., Patlolla, A.K., & Sutton, D.J. (2012). Heavy metals toxicity and environment. *Experientia Supplementum*, 133–164. [https://doi.org/10.1007/978-3-7643-8340-4\\_6](https://doi.org/10.1007/978-3-7643-8340-4_6)
- Tewari, A., Bhutada, D.S., & Wadgaonkar, V. (2023). heavy metal remediation from water/wastewater using bioadsorbents – a review. *Nature Environment and Pollution Technology*, 22, 2039–2053.
- Timmer, K., Van Limpt, H., Fischer, H. (2010) Selenium containing clays minerals as additive for the discoloration of glass. *Applied Clay Science*, 47(3-4), 465–467.
- Viani, A., Gualtieri, A.F., & Artioli, G. (2002). The nature of disorder in montmorillonite by simulation of X-ray powder patterns. *American Mineralogist*, 87, 966–975.
- Villarks, P., & Cenzual, K. (2017). *Pearson's Crystal Data – Crystal Structure Database for Inorganic Compounds*. ASM International, Materials Park, OH, USA.
- Wang, R., Li, H., Ge, G., Dai, N., Rao, J., Ran, H., & Zhang, Y. (2021). Montmorillonite-based two-dimensional nanocomposites: preparation and applications. *Molecules*, 26, 2521.
- Wijitwongwan, R., Intasa-Ard, S., & Ogawa, M. (2019). Preparation of layered double hydroxides toward precisely designed hierarchical organization. *ChemEngineering*, 3, 68.
- Yi, D., Yang, R., & Wilkie, C.A. (2013). Layered double hydroxide-montmorillonite – a new nano-dimensional material. *Polymers for Advanced Technologies*, 24, 204–209.
- Zhang, M., Gao, B., Yao, Y., & Inyang, M. (2013). Phosphate removal ability of biochar/MgAl-LDH ultra-fine composites prepared by liquid-phase deposition. *Chemosphere*, 92, 1042–1047.
- Zigan, F., & Rothbauer, R. (1967). Neutronenbeugungsmessungen am Brucit. *Neues Jahrbuch für Mineralogie Monatshefte*, 137–143.